GEM - International Journal on Geomathematics (2025) 16:18
https://doi.org/10.1007/s13137-025-00275-2

RESEARCH

Mathematical modelling of water absorption properties for historical lime-based mortars

Gabriella Bretti[1] · **Cristina M. Belfiore**[2]

Received: 5 April 2025 / Accepted: 22 September 2025 / Published online: 27 September 2025

Abstract
In this paper we propose a mathematical model of the capillary and permeability properties of lime-based mortars from the historic built heritage of Catania (Sicily, Italy) produced by using two different types of volcanic aggregate, i.e. ghiara and azolo. In order to find a formulation for the capillary pressure and the permeability as functions of the saturation level inside the porous medium we calibrate the numerical algorithm against imbibition data. The validation of the mathematical model was done by comparing the experimental retention curve with the one obtained by the simulation algorithm. Indeed, with the proposed approach it was possible to reproduce the main features of the experimentally observed phenomenon for both materials.

Keywords Mathematical modelling · Numerical simulations · Porous media · Water flow · Absorption properties

1 Introduction

Mortars are among the most widely used artificial building materials due to their many applications in construction. Their main role is to connect masonry elements such as stones and bricks, but they are also used for finishing and aesthetic purposes, as basis for floors, frescoes or mosaics.

Mortars are open porous systems that can be subject to different damaging processes due to the exposure to weathering or chemical aggression. Unfortunately, the deterioration processes of these porous materials caused by the interaction with the environment are still not completely understood, due to the complexity of phenomena involved. Moreover, their composition may vary considerably; indeed, during each historical period, clay, lime, natural pozzolans, brick dust, gypsum or combination of them were used. Most of deterioration processes affecting porous materials are associated to liquid water penetration, either in the form of rain or groundwater moisture

✉ Gabriella Bretti
gabriella.bretti@cnr.it

[1] Istituto per le Applicazioni del Calcolo - CNR, Via Taurini 19, 00185 Rome, Italy

[2] Dipartimento di Scienze Biologiche, University of Catania, Corso Italia 57, 95129 Catania, Italy

infiltration, see for instance (Bretti and Natalini 2023; Charola and Wendler 2015) and references therein.

In this respect, the assessment of the absorption properties of porous materials is crucial to determine the flow of liquid within the pores. This is not an easy task, since mineralogical composition, porosity and pore size distribution can vary even for samples of the same material. Many mathematical models can be found in literature describing the absorption properties of porous materials, see (Assouline 2001; Brooks and Corey 1964; van Genuchten 1980).

In recent papers of one of the authors, the mathematical model describing capillary rise and water imbibition introduced in Clarelli et al. (2009) was applied with promising results to different materials, also in presence of protective treatments, see (Bracciale et al. 2017; Bretti et al. 2021).

In the present paper a mathematical model based on Darcy's law is introduced in order to simulate numerically the water uptake into porous materials. Since we deal with unsaturated flow, the mass balance equation for the liquid (water) having density ρ_l is Bear and Bachmat (1991):

$$\partial_t \theta_l = \partial_z q \tag{1}$$

where θ_l is the *fraction of volume occupied by the fluid* and q is the *volumetric flux*, having the unit measure of a velocity, also called *superficial velocity* of the fluid within the porous medium and it is given by the well known Darcy's law (Bear 1972):

$$q = -\frac{k\left(\frac{\theta_l}{n_0}\right)}{\mu_l}\left(\partial_z P_c\left(\frac{\theta_l}{n_0}\right) - \rho_l g\right). \tag{2}$$

Note that P_c is the capillary pressure, i.e. the pressure drop on the interface between liquid and gas, k is the *relative permeability* of the porous matrix to vapour density, μ_l the *viscosity* of the fluid, n_0 is the open *porosity* of the material, i.e. the fraction of pore volume occupied by voids, while the term $\rho_l g$ takes into account the effect of the gravity in the vertical flow and it can be safely disregarded for small specimens of a given material.

The equation (1) represents a continuity equation describing the variation in time of the fraction of pores occupied by the liquid due to its diffusion in the medium. As usual in literature (Bear and Bachmat 1991; Bear 1972), we assume the capillary pressure as a function of the fluid saturation θ_l/n_0 only, i.e. $P_c = P_c(\theta_l/n_0)$. Then, following the approach in Clarelli et al. (2009), we introduce a function $B(s)$ depending on $s := \theta_l/n_0$, the *water saturation*, i.e. the saturation level within the material, such that $\partial_z B(s) = -\frac{k(s)}{\mu}\partial_z P_c(s)$.

In Clarelli et al. (2009) the absorption function B has a mathematical formulation of a polynomial of third degree with the derivative B' resulting in a concave parabola on a compact support $s \in [s_R, s_S]$, see (11) in paragraph 2.4. In this formulation, derived as an empirical/phenomenological function describing the physical properties of the porous material, there are three crucial parameters: the diffusion rate of water

in the medium, the residual saturation that ensures the hydraulic continuity and the maximum value of saturation.

Here, in order to describe more accurately the physical properties involved in the suction process, we introduce a new formulation of function B, see paragraph 2.5, resulting in a sort of asymmetrical concave parabola where we define separately the capillary pressure function and the permeability function, thus allowing us to derive specific parameters related to the capillary pressure and to the permeability properties of the porous material, that can be calibrated against data. This approach allows us to give a formulation of $P_c(s)$ and $k(s)$ separately; moreover, in this way it is possible to make a validation of the model using the available experimental data, such as permeability test to water vapour (de Boever et al. 2016) and/or MIP (Della Vecchia et al. 2014). Moreover, the model (18) is formulated in such a way to be more adherent to the physical process of imbibition of porous materials with respect to the empirical formulation introduced in Clarelli et al. (2009) and given by formula (11).

Absorption properties of some experimental lime-based mortars are characterized through imbibition experiment with pure water performed in Belfiore et al. (2023). The diffusion coefficient, the residual and maximum value of saturation for the two materials are determined through the numerical calibration of the simpler model in against data - i.e. by computing the difference between model outcomes and experimental data for ghiara and azolo mortars. Then, starting from the results obtained for the simpler model, we calibrate the six parameters of the more sophisticated model against imbibition data getting more accurate results and a complete description of the absorption properties of ghiara and azolo mortars, see Section 3.

The paper is organized as follows: Section 2 is devoted to the description of laboratory experiments on the two lime-based mortars as well as to the presentation of the mathematical model and the related numerical algorithm. Section 3 is concerned with the definition of the inverse problem for the numerical calibration of model parameters and with the validation of the proposed model; moreover, a local sensitivity analysis on the effect of parameters on numerical results is provided. The results are discussed in Section 4. Finally, we end up with conclusions and future perspectives of our research in Section 5.

2 Materials and methods

2.1 The laboratory experiment Belfiore et al. (2023)

The laboratory experiment was carried out on two lime-based mortars replicating those of the historic built heritage of Catania (Eastern Sicily, Italy). These are characterized by two different volcanic aggregates, locally known as azolo and ghiara. Azolo, now obtained from the fine grinding of basalts, in its ancient meaning, was an incoherent pyroclastic rock with grain size ranging from 0.2 to 2 mm, sharp edges, and a dark-gray color (Belfiore et al. 2022). Ghiara is a reddish material deriving from the thermal transformation at highly oxidizing conditions of paleo-soils, originally rich in organic matter, induced by lava flows (Belfiore et al. 2010, 2022).

The experimental mortar specimens have been reproduced in laboratory by following the ancient recipes known from literature (Battiato 1988). The binder used is a ready-made commercial slaked lime with CaO content higher than 90%, MgO in the range 1.5–2%, and solid/water ratio 40:60. As for the volcanic aggregates, after granulometric separation by sieving, the proper amount of each size class to be added to the mixture was determined by using the Fuller's particle size equation. The maximum grain size used for aggregates was 2 mm, while the aggregate/binder ratio per volume was 2:1 in both mortar types. The formulations were prepared by mixing binder and aggregates with a proper amount of water (3 vol% in the ghiara mortar and 5 vol% in the azolo one) to achieve adequate workability. A mechanical mixer was used for a better homogenization of the mixture which was then poured into 5x5x5 cm molds. A vibrating table allowed removing air bubbles thus favoring the packaging. The specimens have been demolded after 7 days and left curing for further 21 days at room temperature (25°C) by keeping the relative humidity level at about 80-85%. The two replicated mortars were designed in Belfiore et al. (2023) to assess their physical-chemical durability. For that purpose, the authors used a multi-analytical approach including mineralogical-petrographic and physical investigations (polarized optical microscopy, X-ray diffraction, pore size distribution, water absorption by capillarity, water vapor permeability), along with accelerated aging tests by salt crystallization and sulfur dioxide attack. The data of capillary water absorption test, here used for the mathematical modelling, were determined according to the European standard UNI EN 1015-18 (2004). Specifically, three specimens per each mortar type were placed inside a ventilated oven for 24 h to remove residual moisture and after that the dry weight of each sample was calculated. Then, the specimens were placed inside a container with the lower face immersed in about 5–10 mm of water and covered to prevent water evaporation. After 10 min, the specimens were extracted from the basin and weighted (M1), then again immersed and after 90 min weighted to obtain the final mass (M2).

The amount of absorbed water (Q_i) was measured as follows:

$$Q_i = (w_i - w_0)/A,$$

where: w_i and w_0 are the weights (in g) of the sample at times t_i and t_0, respectively; A (cm^2) is the area of the surface exposed to water. See Fig. 1 for the experimental setup of the imbibition test.

2.2 MIP experiment

The experimental test used to have quantitative information on the pore size distribution of porous media with interconnected porosity is the mercury intrusion porosimetry (MIP). Specifically, pores in the range 0.005–750 μm were analyzed by using a Micromeritics Autopore V 9600 porosimeter reaching a maximum pressure of 227 MPa (Belfiore et al. 2023).

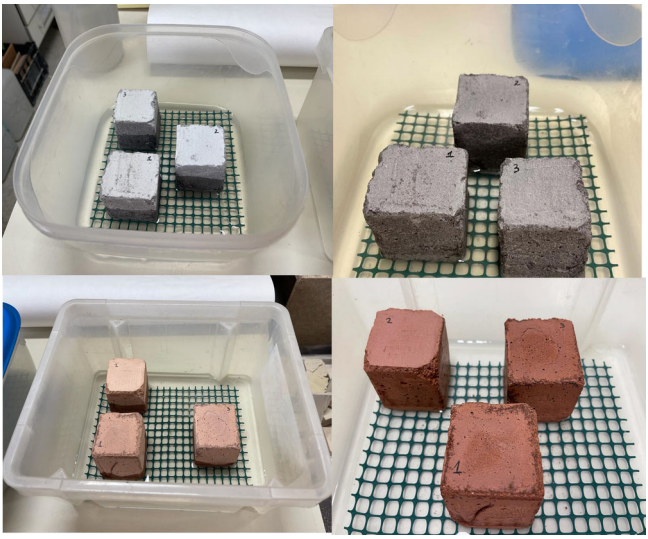

Fig. 1 Laboratory experiment for the measurement of water absorption for azolo (top) and ghiara (bottom) mortars

By using information provided by MIP, water retention models can be developed, see (Della Vecchia et al. 2014) and references therein.

Suction is computed from MIP data using Laplace formula reported in Cardoso et al. (2022). In particular, the capillary pressure, P^i_{MIP}, can be computed directly from mercury pressure, P^i_{Hg} corresponding to saturation level s^i_{Hg}, using the Laplace equation:

$$P^i_{MIP} = \frac{T_w \cos(\theta_w)}{T_{Hg} |\cos(\theta_{Hg})|} P^i_{Hg}, \tag{3}$$

with $i = 1, \ldots, N_{MIP}$ the number of MIP measurements, T_w and T_{Hg} the surface tensions of water and mercury, respectively ($T_w = 0.073 N/m$ and $T_{Hg} = 0.489 N/m$); and θ_w and θ_{Hg} the contact angles of water and mercury, respectively, $\theta_w = 0°$ and $\theta_{Hg} = 130°$. We remark that here we express the capillary pressure in the unit measure $[g/(cm \cdot s^2)]$.

Notice that the saturation level $s_{Hg,i}$ is obtained from MIP data as:

$$s_{Hg,i} = 1 - V_i / V_{max}, \; i = 1, \ldots, N_{MIP},$$

with V_i and V_{max}, respectively, the specific and the maximum specific volume of pores.

2.3 The mathematical model of suction of pure water

We denote the fraction of volume occupied by the liquid and by the gas (composing the fluid) within the representative element of volume, respectively by θ_l and θ_g. The open porosity n_0 of unperturbed material satisfies the following relation:

$$n_0 = \theta_l + \theta_g. \tag{4}$$

Since we are considering specimens of small dimension, gravity effects can be safely neglected in Darcy's law. Then, we introduce a function B describing the absorption properties of porous material so that Darcy's law (2) can be rewritten as

$$q = \partial_z B(s) = -\frac{k(s)}{\mu}\partial_z P_c(s). \tag{5}$$

The identification of the function B reproducing the capillary rise properties of a specific porous material is not an easy task. Indeed, there are many suggested experimental curves aiming to connect the capillary pressure with the moisture content, but they are not completely reliable since a relation correlating capillary pressure with moisture content into the porous matrix still lacks. There are many possible choices for the function $B(s)$, since it can vary very much according to the physical property of any given material. A simple and phenomenological description of the capillary rise of water can be obtained by defining B as a compactly supported function in order to reproduce the fact that the liquid (water) flows within the material only if the saturation s ranges between a minimum and maximum saturation level, with a diffusion rate to be calibrated against experimental data. Two possible formulations of B', i.e. "concave parabola" and "asymmetrical concave parabola" are proposed, respectively, in the next paragraphs 2.4 and 2.5, see also pictures in Fig. 3. From now on, for the sake of simplicity, we suppress the label l. Then, the one-dimensional mathematical model for the experiment of imbibition given by (1) can be written as:

$$\partial_t \theta = \partial_{zz} B(s), \tag{6}$$

with B the function satisfying relation (5).

Equation (6) has to be coupled with reasonable initial and boundary conditions. We assume the following initial and boundary conditions

$$\theta(z, 0) = 0, z \in [0, h_1] \tag{7}$$
$$\theta(z, t) = n_0, z \in [0, h_2], t \in [0, T_f] \tag{8}$$
$$\theta(h_1, t) = \bar{\theta}, t \in [0, T_f], \tag{9}$$

with h_2 the height of the immersed part, meaning that the bottom side of the sample is always saturated since it is placed in direct contact with water, while at the top side $z = h_1$ the condition (9) reproduces the exchange of the specimen with the humidity within the bucket ($\bar{\theta}$ is the moisture content of the ambient air) due to evaporation,

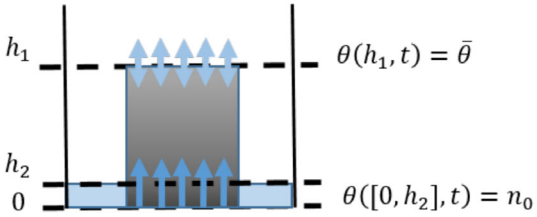

Fig. 2 Schematic representation of boundary conditions reproducing the laboratory experiment of water absorption by capillary rise in the specimen and reported in (8)-(9)

thus we assume it as the value of humidity on the facelet on the top of the material. In the above condition, $\bar{\theta}$ is assumed constant during the experiment. For the sake of clarity, we report a schematic representation of the domain in Fig. 2.

2.3.1 Remark

The Dirichlet boundary condition at the top boundary can be replaced by the Robin boundary condition:

$$\partial_z \theta(L, t) = K_w(\bar{\theta} - \theta(L, t)),$$

in order to reproduce the exchange of water occurring gradually at the upper boundary $z = L$, being regulated by the condition on the derivative $\partial_z \theta$, with a rate given by a coefficient $K_w > 0$. More specifically, if $(\bar{\theta} - \theta(L, t)) > 0$ the water vapour penetrates from the outer boundary within the material and the derivative increases; on the contrary if $\bar{\theta} < \theta(L, t)$ then water in the material evaporates and the derivative on the right boundary is negative. Even if this condition seems to be more realistic, here we prefer to use a Dirichlet boundary condition in order to reduce the number of model parameters to be calibrated. Note that, for large values of K_w the solutions obtained numerically assuming Robin boundary conditions seem to converge towards those with Dirichlet ones.

Since in this experimental settings the evaporation from lateral sides is negligible, then in this in one-dimensional formulation we did not include it in (5). Note that to get $\bar{\theta}$ we used formula for the saturated vapor density (SVD in $[g/m^3]$) as function of temperature T [C]:

$$SVD(T) = (5.018 + 0.32321T + 8.1847 \times 10^{-3}T^2 + 3.1243 \times 10^{-4}T^3) \times 10^{-6},$$

from which we can obtain the density of vapor in $[g/cm^3]$.

The value of $\bar{\theta}$ is obtained from the formula [24]:

$$\bar{\theta} = SVD(T) \cdot \frac{UR}{100}, \tag{10}$$

where $T = 25°C$ and $UR = 90\%$ is the percentage of humidity in the ambient air, see Table 2 for the values of the parameters of the problem.

In the following, we propose two possible formulations for B function.

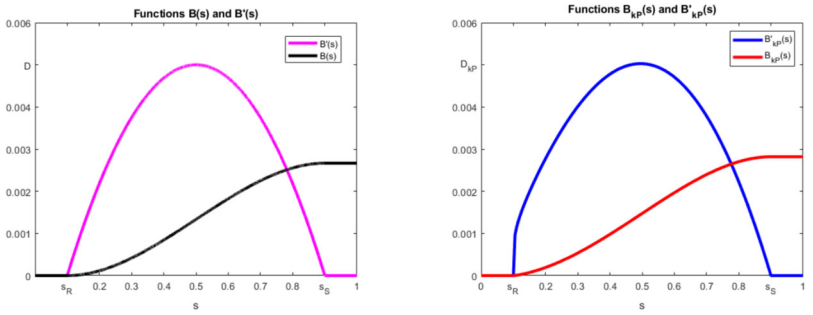

Fig. 3 Left panel: Plot of functions $B(s)$ and $B'(s)$ defined in formula (11) and obtained for $s_R = 0.1$, $s_S = 0.9$ and D =5e-03. Right Panel: Plot of functions $B(s)$ and $B'(s)$ defined in formula (18) and obtained for $s_R = 0.1$, $s_S = 0.9$, $\alpha = 0.25$, c =1.35e+05, K_s = 8e-10,$\gamma = 1.45$ with D_{kP} =5e-03

2.4 The absorption function B' (Clarelli et al. (2009))

Here, among the possible choices for B function, a possible formulation is the function first introduced in Clarelli et al. (2009):

$$B(s) = \begin{cases} 0 & s \in [0, s_R) \\ -\frac{(2D(s_R - s)^2(s_R - 3s_S + 2s))}{3(s_R - s_S)^2} & s \in [s_R, s_S] \\ \frac{2}{3}D(s_S - s_R) & s > s_S, \end{cases} \tag{11}$$

$$\text{with } \partial_s B(s) = B'(s) = max\left(0, -\frac{4D(s_R - s)(s_S - s)}{(s_R - s_S)^2}\right), \tag{12}$$

and $\{s_R, s_S, D\}$ is the set of model parameters to be determined: s_R, the minimum value for saturation ensuring the hydraulic continuity, s_S the maximum value of s reached at saturation, and the maximum value $D = \max_{[s_R, s_S]} B'$ reached at $s = \frac{s_R + s_S}{2}$. We remark that $B'(s)$ is a compactly supported function for s in $[s_R, s_S]$ and D has the dimensions of a diffusivity. Then, the profiles of $B(s)$ and $B'(s)$ are obtained by letting the right and left endpoints s_R and s_S vary, i.e. $s_S > s_R > 0, s_S \leq 1$, meaning that the realistic pore saturation is normally less than 100%. An example of the profiles of B and B' can be found in the left panel of Fig. 3.

Remark 1 It is worth noting that, due to its simplicity, this formulation of B and B' has the great advantage of depending only on 3 parameters, thus it is quite easy to be calibrated against data. However, here we do not have the possibility of expressing the capillary pressure P_c and the permeability function $k(s)$ independently as in Darcy's law (5). From a modelling point of view, the model (11) can be considered as a phenomenological/empirical model.

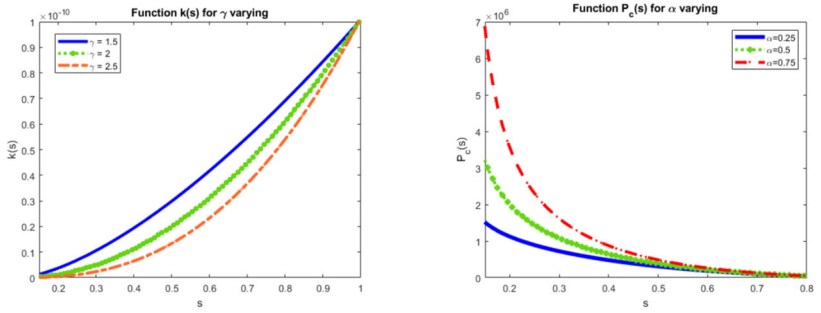

Fig. 4 Plot of permeability function (13) for K_s =1e-10 and of capillary function (14) for fixed c =1e+06, assuming different values of α

2.5 A new formulation of absorption function B' for Darcy's law

A slightly different formulation of function B in Darcy's law (5) that conserves the main features of function B described in (11) and allows us to express separately the permeability function $k(s)$ and the capillary pressure $P_c(s)$ is introduced. In particular, the permeability function $k(s)$ is formulated in such a way to reproduce the profile described in Chapter 9 of Bear (1972), i.e the permeability is a monotonic function increasing with s. Then it is expressed as:

$$k(s) = \begin{cases} K_s \left(\frac{s-s_R}{s_S-s_R}\right)^{\gamma}, & \text{if } s \in (s_R, s_S), \\ 0, & \text{if } s \in [0, s_R], \\ K_s, & \text{if } s \in [s_S, 1], \end{cases} \tag{13}$$

with $K_s > 0$ the constant of permeability at saturation, possibly obtained by experimental measurements, and $\gamma > 0$ a parameter to be calibrated with experimental data. For the capillary pressure, a possible formulation qualitatively reproducing the profile reported in Bear (1972); Della Vecchia et al. (2014), is:

$$P_c(s) = c\frac{(s-s_S)^2}{(s-s_R)^{\alpha}}, \quad \text{if } s \in (s_R, s_S], \tag{14}$$

with $c > 0$ a characteristic coefficient for the given material, s_R and s_S the saturation parameters defined above and $\alpha \in (0, 1)$ an exponent to be calibrated against data. More in details, function $P_c(s)$ has the following behavior: $P_c(s_S) = 0$ and it tends to infinity for $s \to s_R$. The derivative $\partial_s P_c = P_c'(s)$ is then:

$$P_c'(s) = -\frac{c(s-s_S)(2s_R - 2s - \alpha s_S + \alpha s)}{(s-s_R)^{\alpha+1}}. \tag{15}$$

As an example, we depict in Fig. 4 the profile of functions (13) and (14) obtained for different parameters.

Then, keeping the same framework introduced in the previous paragraph we consider B' as a compactly supported function in $[s_R, s_S]$. We introduce this new formulation using (13) and (15) in (5) so that we get the following expression for the derivative $\partial_s B_{kP}$ called for simplicity $B'_{kP}(s)$:

$$B'_{kP}(s) = \begin{cases} 0 & s \in [0, s_R] \cup [s_S, 1] \\ max\left(0, K_s \frac{c}{\mu} \frac{(s-s_R)^{\gamma-\alpha-1}}{(s_S-s_R)^{\gamma}}(s-s_S)(2s_R + s(\alpha-2) - \alpha s_S)\right) & s \in (s_R, s_S). \end{cases} \tag{16}$$

In this case the set of model parameters is given by $\{s_R, s_S, \alpha, c, K_s, \gamma\}$, with $\gamma - \alpha - 1 > 0$ and we indicate by $D_{kP} = \max_{[s_R,s_S]} B'_{kP}$ the diffusion coefficient. Now, we integrate exactly $B'_{kP}(s)$ from (16), and we get the following expression:

$$\widetilde{B}_{kP}(s) = \frac{K_s c (s-s_R)^{\gamma-\alpha}}{\mu(s_S-s_R)^{\gamma}} \cdot \cdot \frac{s^2 u + sv + \gamma^2 s_S(-2s_R + \alpha s_S) + \gamma z + \alpha s_S^2(\alpha^2 - 3\alpha + 2)}{(-\alpha^3 + 3\alpha^2(\gamma+1) - 3\alpha\gamma(\gamma+2) - 2\alpha + \gamma^3 + 3\gamma^2 + 2\gamma)}, \tag{17}$$

with

$$u = \alpha^3 - \alpha^2(2\gamma+3) + \alpha(5\gamma+2) - 2\gamma(\gamma+1),$$
$$v = 2\gamma(-s_R\alpha + 2\alpha^2 s_S + 2s_S - 4\alpha s_S) + 2\gamma^2(s_R - \alpha s_S + s_S) + 2\alpha s_S(-\alpha^2 + 3\alpha - 2),$$
$$z = 2s_R^2 + \alpha s_S^2(-2\alpha + 3) + 2s_R s_S(\alpha - 2),$$

and we introduce the coefficient $C = K_s c$.

Then, $B_{kP}(s)$ reads as:

$$B_{kP}(s) = \begin{cases} 0 & s \in [0, s_R] \\ \widetilde{B}_{kP}(s) \text{ in (17)} & s \in (s_R, s_S) \\ \widetilde{B}_{kP}(s_S) = \frac{2K_s c\gamma(s_S-s_R)^{2-\alpha}}{\mu(-\alpha^3+3\alpha^2(\gamma+1)-3\alpha\gamma(\gamma+2)-2\alpha+\gamma^3+3\gamma^2+2\gamma)} & s \in [s_S, 1]. \end{cases} \tag{18}$$

An example of the profiles of $B_{kP}(s)$ and $B'_{kP}(s)$ can be found in the right panel of Fig. 3.

3 Calibration and validation of the mathematical model: statement of the inverse problem and results

Now we describe the calibration procedure to determine parameters of the imbibition function (16) using the experimental data of imbibition experiment both for ghiara

and azolo mortars. The objective is to reproduce numerically the cumulative water absorption, i.e. the water that crosses the mortar samples by capillary suction.

3.1 Calibration of imbibition parameters in (18) against data

We calibrate model parameters in two steps:

Step 1. First we calibrate model parameters, i.e. saturation parameters s_R, s_S and the diffusion coefficient D, in the simpler model (11) against data by finding those that minimize the error (20). In this way we gain insights on the order of magnitude of the diffusive physical phenomenon corresponding to $\max_{[s_R,s_S]} B'(s)$ and the initial guess for s_R, s_S.

Step 2. Then, for the calibration of the model (18) we look for the set of parameters minimizing the difference (20) between data and simulation outcomes proceeding as follows:

- we assume the values obtained at the end of Step 1 for s_R and s_S as initial guess and we let them vary slightly;
- we tune the other model parameters in B_{kP}, namely α, c, K_s and γ, in such a way that D_{kP} has the same order of magnitude of the diffusion coefficient D obtained in Step 1.

Finally, we validate our results by comparing the capillary pressure profile in (14) using optimal parameters found with the procedure above with MIP data described in 2.2.

Definition of the error between data and model outcome. In order to calibrate parameters of absorption function B' we need a measure to establish a comparison between model outcomes and data coming from the experiment of water imbibition. Since the relevant quantity that is experimentally accessible is the total quantity of water Q_k absorbed by the specimen at certain scheduled time intervals t_k, we compute the total amount of fluid absorbed obtained by the numerical algorithm at the same time intervals (Q_k^{num}), as explained below. First we make a discretization in time and space of the computational domain: $z_j = j\Delta z$, $j = 0, ..., N = \left[\frac{h_1}{\Delta z}\right]$, $\{t_k\}_{k=1,...,N_{meas}}$, and we define the water content on the numerical grid as $\theta_j^k = \theta(z_j, t_k)$. Then, we solve numerically equation (6) coupled with the boundary conditions (8)-(9) in order to get the water content, by using the explicit forward in time-central in space approximation scheme (Aregba-Driollet et al. 2004):

$$\theta_j^{k+1} = \theta_j^k + \frac{\Delta t}{\Delta z^2}(B(\theta_{j+1}^k/n_0) - 2B(\theta_j^k/n_0) + B(\theta_{j-1}^k/n_0)), \tag{19}$$

where B is the absorption function either defined in (11) or (18) under the CFL condition

$$\frac{\Delta t}{\Delta z^2} \leq \frac{n_0}{2\max_{[s_R,s_S]} B'(s)}.$$

Table 1 Physical parameters of the porous materials

Parameter	Description	Units	Value	Ref.
n_0	open porosity of ghiara mortar	-	4.66e-01	exp. data
n_0	open porosity of azolo mortar	-	3.85e-01	exp. data
τ	tortuosity factor of ghiara mortar	-	9.9	exp. data
τ	tortuosity factor of azolo mortar	-	7.6	exp. data

At the bottom boundary we assume the imbibition condition $\theta_0^{k+1} = n_0^{k+1}$, and at the top boundary we use the exchange condition: $\theta_{N+1}^{k+1} = \bar{\theta}$.

Then, we get the quantity of water in the specimen at time t_k obtained by the numerical algorithm by approximating the integral $\int_0^{h_1} \rho\theta(z, t_k)dz$, with ρ the density of water, by using the trapezoidal rule:

$$Q_k^{num} = \rho\frac{\Delta z}{2}\left(\theta_0^k + 2\sum_{j=1}^{N-1}\theta_j^k + \theta_N^k\right),$$

in order to compare model outcome with experimental data at the same times. The error to be minimized is then defined as the sum of all the relative square errors between experimental data and numerical simulation Tables 1 and 2:

$$E_{1,2} = \frac{1}{N_{meas}}\sum_{k=1}^{N_{meas}}\frac{(Q_k^{num} - Q_k)^2}{(Q_k^{num})^2}, \tag{20}$$

with E_1 depending on the set of parameters $\{s_R, s_S, D\}$ and E_2 depending on $\{s_R, s_S, \alpha, c, K_s, \gamma\}$, for the functions B' and B'_{kP}, respectively. The calibration procedure has been carried out in MATLAB© applying the simulated annealing method; the optimal parameters obtained for the absorption functions (11) and (18) are reported in Table 3 and 4, respectively. The computational time for a single simulation with fixed parameters takes about 3 seconds for the simpler model (11) and 120 seconds for the model (18) on an Intel(R) Core(TM) i7-3630QM CPU 2.4 GHz assuming as space step $\Delta z = 2.5\text{e-}02$ and time step $\Delta t = 3.5\text{e-}02$. In Table 5 are listed the results obtained by the absorption function (11) and (18).

3.2 Numerical order of convergence

Now, in order to assess the numerical order of convergence of the numerical method (19), we approximate the problem (6)-(8)-(9)-(18) assuming as model parameters the values obtained for azolo mortar in Table 4. Then we compare the numerical orders

Table 2 Fixed parameters/experimental setup given in input of the mathematical model (6)-(8)-(9)

Parameter	Description	Units	Value	Ref.
$\bar{\theta}_l$	moisture content of the ambient air	-	2.1e-03	eq. 10
h_1	sample's height	cm	5.0	exp. data
h_2	sample's height immersed	cm	2.5e-02	assumption
ρ_l	density of water	g/cm^3	1	Chen et al. (2006)
μ	water viscosity at 25°	Poise	8.9e-03	Rumble (2018)
T_f	final observation time	s	5400	exp. data

Table 3 Parameters obtained with a fitting procedure for B function (11)

Ghiara mortar			
Parameter	Description	Units	Value
s_R	residual saturation	-	6.75e-01
s_S	max. saturation level	-	1.0
D	diffus. coeff. in (11)	cm^2/s	1.95e-02
Azolo mortar			
Parameter	Description	Units	Value
s_R	residual saturation	-	5.21e-01
s_S	max. saturation level	-	1.0
D	diffus. coeff. in (11)	cm^2/s	4.8e-03

of convergence, defined as follows

$$\gamma = \log_2 \left(\frac{E(\Delta z, \Delta t)}{E(\frac{\Delta z}{2}, \frac{\Delta t}{2})} \right), \tag{21}$$

where

$$E(\Delta z, \Delta t) = \Delta z \sum_{j=0}^{N} \left| \theta_j^T(\Delta z) - \theta_{2j}^T \left(\frac{\Delta z}{2} \right) \right|, \tag{22}$$

is the L^1-error, with $\theta_j^T(\Delta z)$ denotes the numerical solution obtained for the discretization space step Δz and computed in x_j at final time Table 6.

The table above shows that the numerical order of convergence of the forward in time-central in space scheme is 1.

3.3 Validation of the calibration procedure using MIP data

Here we validate our procedure by comparing the model outcomes obtained for calibrated model parameters against MIP data described in paragraph 2.2, by using the

Table 4 Parameters obtained with fitting procedure for B_{kP} function (18)

Ghiara mortar			
Parameter	Description	Units	Value
s_R	residual saturation	-	6.75e-01
s_S	max. saturation level	-	9.994e-01
c	characteristic coeff.	$g\ cm^{-1}s^{-2}$	1.4e+06
α	exponent in (18)	-	0.25
K_s	permeability at satur.	cm^2	7.65e-10
γ	curvature parameter in (18)	-	1.865
D_{kP}	diff. coeff. in (18)	cm^2s^{-1}	1.97e-02
Azolo mortar			
Parameter	Description	Units	Value
s_R	residual saturation	-	5.5e-01
s_S	max. saturation level	-	1e-01
c	characteristic coeff.	$g\ cm^{-1}s^{-2}$	1.98e+05
α	exponent in (18)	-	0.25
K_s	permeability at satur.	cm^2	7.93e-10
γ	curvature parameter in (18)	-	1.45
D_{kP}	diff. coeff. in (18)	cm^2s^{-1}	4.84e-03

Table 5 Error values E_1 and E_2 defined in (20) and obtained, respectively, by the absorption function (11) and (18)

Material	Error Value E_1	Error Value E_2
ghiara mortar	2.20e-04	1.45e-04
azolo mortar	1.44e-04	1.22e-04

Table 6 Numerical order of convergence defined in (21) of the approximation scheme

Δx	Order of the scheme
0.5	1.0054
0.25	1.0071
0.125	1.0076
0.0625	1.0070

formulation of the capillary pressure function reported in (14). In particular, in Figs. 5 and 6 are reported the profiles of the experimental water retention curve and of the numerical one obtained with model (18) using optimal parameters in Table 4.

It is worth noting that the superposition between the water retention curve derived from experimental data and that obtained by the mathematical model is used here as a qualitative and only partially quantitative comparison. Indeed, our aim is to assess the order of magnitude of the capillary pressure values obtained from MIP experiment. In this way we can verify that model parameters obtained in the calibration procedure

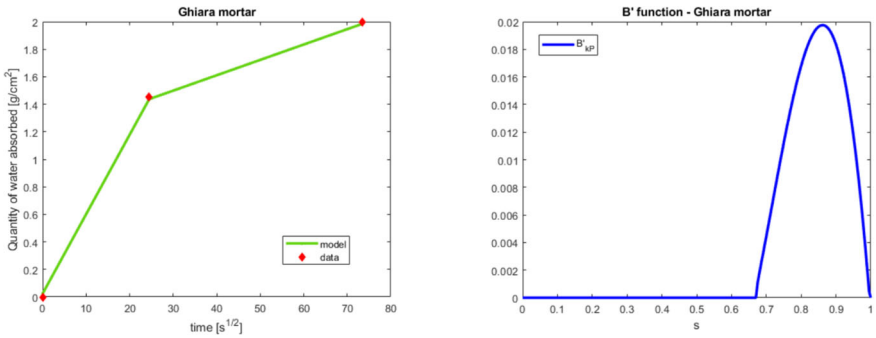

Fig. 5 Left panel: Plots of the imbibition curve for ghiara mortar obtained numerically by the mathematical model (6)-(8)-(9)-(18) (green line) VS experimental data (red diamonds). Right panel: Plot of B' function (18) for ghiara mortar (blue line)

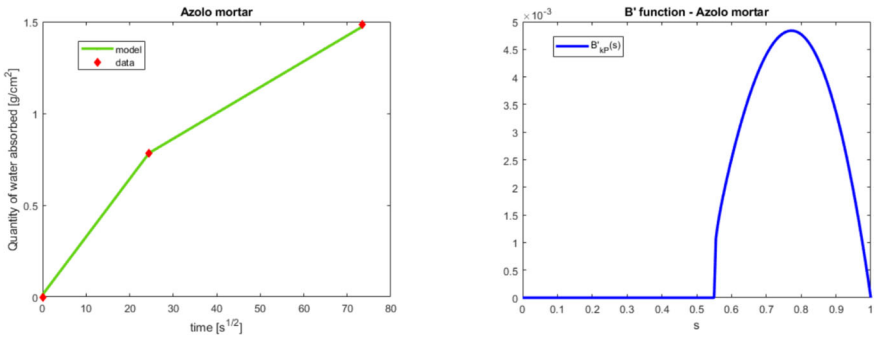

Fig. 6 Left panel: Plot of the imbibition curve for azolo mortar obtained numerically by the mathematical model (6)-(8)-(9)-(18) (green line) VS experimental data (red diamonds). Right panel: Plot of B' function (18) for azolo mortar (blue line)

described in paragraph 3.1 allow us to get values of $P_c(s)$ that are in accordance with experimental data, as shown for both materials in Figs. 7 and 8.

3.4 Sensitivity analysis

In the present Section we perform a sensitivity analysis that explores the space of parameter values in which the mathematical problem is set, so that the effects of single parameters on the dynamics can be evaluated. In the model (18) there are 6 parameter values that strongly affect model outcomes in terms of the quantity of water absorbed by the specimen across time. Specifically, here we compute the error functional E_2 defined in (20) and obtained by changing in turn only one parameter keeping the other fixed, i.e. one factor-at-time (OAT) procedure. Then, we observed that error functional E_2 is strictly related to the variation of parameter values and we verified that the optimal parameters obtained by the fitting procedure correspond to the minimum values of the error functionals, as expected. The results of the local sensitivity analysis on model parameters are reported in Figg. 9 and 10.

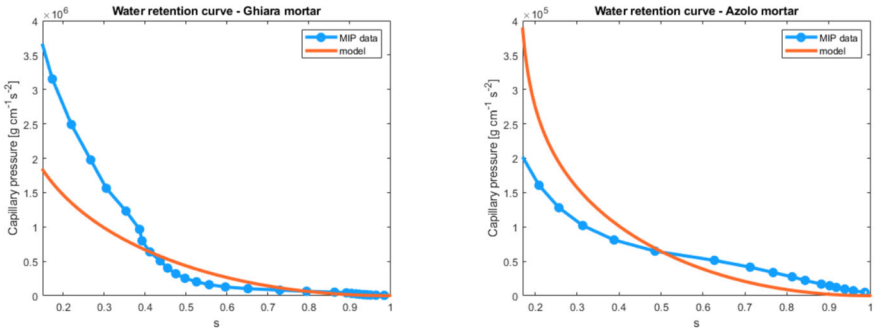

Fig. 7 Left Panel: Plot of water retention curve for ghiara mortar. Experimental data (blue dotted line) VS curve profiles obtained numerically by the two models for capillary pressure $P_c(s)$, reported in (14) for $\alpha = 0.25, c = 1.4e{+}06$ (orange line). Right Panel: Plot of water retention curve for azolo mortar. Experimental data (blue dotted line) VS curve profiles obtained numerically by the two models for capillary pressure $P_c(s)$, reported in (14) for $\alpha = 0.25, c = 1.98e{+}05$ (orange line)

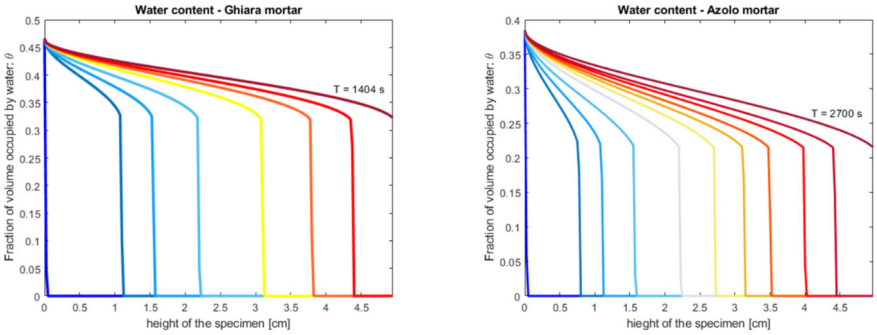

Fig. 8 Plot of the water content as a function of length at different times during imbibition obtained numerically for ghiara (left panel) and azolo (right panel)

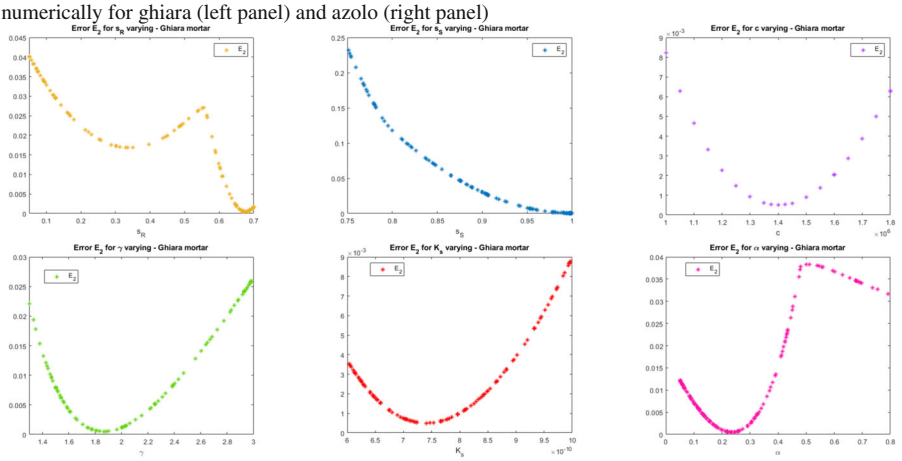

Fig. 9 Local sensitivity analysis with respect to model parameters for ghiara mortar: plots of the error functional E_2

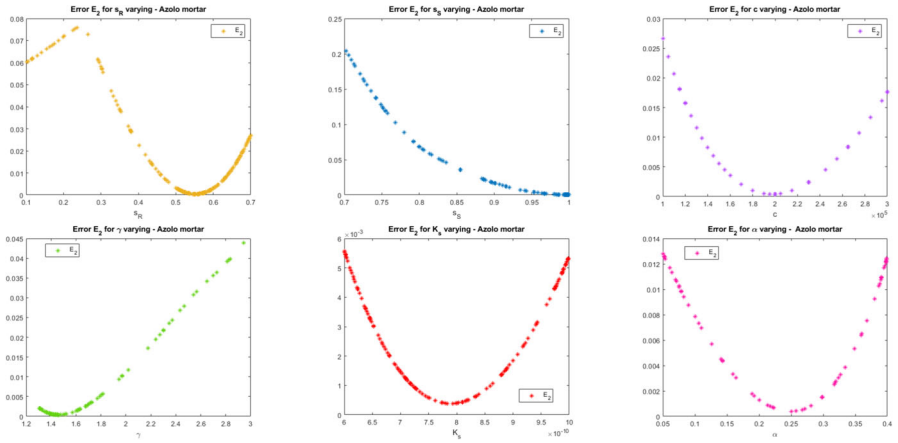

Fig. 10 Local sensitivity analysis with respect to model parameters for azolo mortar: plots of the error functional E_2

4 Discussion of results and methodology

From the results reported in Section 3.1 and 3.3, we can see that water diffuses more rapidly in ghiara mortar respect to azolo one. Indeed, the diffusion coefficient D_{kP} for ghiara mortar is about 4 times greater, as shown in Table 4. As a consequence, the water fills in the pores more rapidly in ghiara mortar, as can be seen from the profiles of water θ within the pores across time reported in Fig. 8 along the specimen's heights. Then, the liquid in ghiara mortar reaches the sample's top more rapidly than in azolo one. Indeed, the water reaches the top of the specimen at time $T = 2700\ s$ (about 45 mins) for azolo mortar, while for ghiara mortar the top is reached at a shorter time $T = 1404\ s$ (about 23 mins). This seems to be in accordance with the experimental data (Belfiore et al. 2023): it can be seen that the imbibition curve reported in the left panel of Fig. 5 in its initial part, i.e. until the first timepoint (10 mins), has a steepest slope with respect to the curve profile in the left panel of Fig. 6.

Conversely, from 10 to 90 mins, the slope of imbibition curve of azolo mortar appears to be slightly steepest than that of ghiara mortar. This unlike behavior at different times can be justified by the fact that at the beginning of the test the ghiara mortar tends to absorb water more quickly due to its greater number of pores (its open porosity found by the MIP analysis is in fact higher, i.e. 46.6% vs. 38.5%, see Table 1). However, it is also characterized by a more complex pore geometry with respect to azolo mortar and this, at a later time, causes in such a specimen a higher decrease in diffusive transport resulting from convolutions of the flow paths through porous media. Such assumption is supported by the "tortuosity" (τ) values obtained from MIP analysis of the two mortar types analyzed in Belfiore et al. (2023) and reported in Table 1. More specifically, tortuosity is a parameter characterizing the geometry and length of interconnected phases. In porous media, it is defined as the ratio of the actual length of the flow-path divided by a straight line length in the direction of flow (Backeberg et al. 2017). The value τ of the two mortar specimens, as reported in Table 1, is 7.6 for

azolo and 9.9 for ghiara, which is in accordance with the above observations. The final quantity of adsorbed water found by the mathematical model resulted to be higher in the ghiara mortar (2 g/cm^2) than in the azolo one (1.5 g/cm^2), even in this case fitting well the experimental data. Such a higher water content absorbed by the ghiara mortar can be again justified by its higher open porosity.

From the computational point of view, the numerical algorithm based on the simpler absorption model (11) has two great advantages: on one hand, the running time is much lower respect to the numerical algorithm based on the model (18); on the other hand the calibration procedure is more easily accomplished since there are only 3 parameters to be calibrated. Both absorption models (11) and (18) are able to reproduce quite well the phenomena observed experimentally, as can be seen from the values of errors obtained for optimal parameters and reported in Table 5. However, it can be noticed that the error values E_2 are less than E_1 for both materials, see Table 5. Moreover, it is worth to note that the absorption model (18) provides a deeper understanding on the permeability properties and capillary pressure of porous materials, since it provides the mathematical formulation of the permeability function as well as of the capillary pressure. For this reason, it allows us to have a validation of the model against experimental MIP data and permeability data, when available.

In this case, the experimental data of permeability at saturation was not available, then the value of K_s was obtained from the numerical calibration of the model by using data at our disposal. We point out that the value obtained for K_s is of order of magnitude of $10^{-10} cm^2$ for both materials and thus falls within the ranges of values reported in literature for the material composing the mortars (i.e. lime, basalts and igneous rocks), see Fig. 1 in Gleeson et al. (2011). This result is qualitatively in accordance with the experimental findings in Belfiore et al. (2023), where the water vapor permeability test showed a similar behavior for the two mortars with only negligible differences between them.

5 Conclusions and future perspectives

In the present work we calibrated and validated a new mathematical model in order to describe the water absorption properties of two lime-based materials of the historic built heritage of Catania, i.e. ghiara and azolo mortars. The fitting procedure showed the effectiveness of our modelling approach, since we were able to simulate the amount of water absorbed by the specimen across time in accordance with imbibition data and to reproduce numerically the behavior of water retention curve derived from MIP data as well. More in detail, we reproduced the imbibition curve with an average percentage error of about 0.01-0.02%.

A validation of our modelling was possible by comparing the water retention curve obtained by the numerical algorithm against curves computed from MIP data. In the future we aim at investigating further aspects both from the experimental and mathematical point of view. From the experimental point of view we are interested in repeating the experiment of water imbibition for a longer observation time and applying protective treatments to the specimen made of ghiara and azolo mortars in order to see how the absorption properties change.

From the mathematical viewpoint we will study the behavior of the models for water absorption here considered in comparison with classical models and we will apply them to different porous materials. Moreover, we will make a rigorous and systematic analysis of the effects of each model parameter on the numerical solution. To this aim, in forthcoming works we will apply both theoretical methods and computational techniques of statistical inference to analyze the effect of the variation of model parameters on model outcomes.

Acknowledgements G. B. is a member of the Gruppo Nazionale Calcolo Scientifico-Istituto Nazionale di Alta Matematica (GNCS-INdAM). She is involved in PRIN project MATHPROCULT Prot. P20228HZWR, CUP J53D23015940001. G.B. is in the PNRR Project H2IOSC CUP B63C22000730005, financed by European Union-NextGenerationEU PNRR Mission 4, "Instruction and Research"-Component 2-Investment line 3.1. G. B. and C. M. B. are in Project PE0000020 CHANGES-CUP [CNR: B53C22003890006, UNICT: E63C22001960006], NRP Mission 4 Component 2 Investment 1.3, Funded by the European Union-NextGenerationEU under the Italian Ministry of University and Research (MUR).

Author Contributions G.B. Conceptualization, Methodology, Software, Validation, Formal analysis, Investigation, Resources, Data Curation, Writing-Original Draft, Writing-Review & Editing, Visualization, Supervision, Project administration, Funding acquisition. C.M.B. Validation, Investigation, Writing-Original Draft, Writing-Review & Editing, Funding acquisition. All authors reviewed the manuscript.

Funding Open access funding provided by Consiglio Nazionale Delle Ricerche (CNR) within the CRUI-CARE Agreement.

Data Availability Data are taken from the published article cited in our manuscript: "C. M. Belfiore, G. Montalto, C. Finocchiaro, G. Cultrone, P. Mazzoleni. Durability tests on lime-based mortars from the historic built heritage of Catania (Eastern Sicily, Italy): An experimental study. Journal of Building Engineering 80 (2023) 108137."

Declarations

Competing interests The authors declare no competing interests.

References

http://www.groundwatersoftware.com/v9_n9_vistas.htm

Andrade, C., d'Andréa, R., Rebolledo, N.: Calculation of tortuosity factor for the model based in concrete resistivity, (2012)

Assouline, S.: A model for soil relative hydraulic conductivity based on the water retention characteristic curve. Water Resour. Res. **37**, 265–271 (2001)

Bear, J., Y. Bachmat, Y.: Introduction to modelling of transport phenomena in porous media, Kluwer Academic Publisher, (1991)

Belfiore, C.M., Montalto, G., Finocchiaro, C., Cultrone, G., Mazzoleni, P.: Durability tests on lime-based mortars from the historic built heritage of catania (eastern sicily, italy): an experimental study. Journal of Building Engineering **80**, 108137 (2023)

Bretti, G., De Filippo, B., Natalini, R., Goidanich, S., Roveri, M., Toniolo, L.: Modelling the effects of protective treatments in porous materials, Mathematical Modeling in Cultural Heritage. In: (a cura di): E: Bonetti, C. Cavaterra, R. Natalini, M. Solci., Mathematical Modeling in Cultural Heritage. SPRINGER INDAM SERIES, p. 73-83, ISBN: 978-3-030-58076-6, ISSN: 2281-518X. (2021)

Bracciale, M.P., Bretti, G., Broggi, A., Ceseri, M., Marrocchi, A., Natalini, R., Russo, C.: Crystallization inhibitors: explaining experimental data through mathematical modelling. Appl. Math. Model. **48**, 21–38 (2017). https://doi.org/10.1016/j.apm.2016.11.026

Bretti, G., Natalini, R.: Forecasting damage and consolidation: Mathematical models of reacting flows in porous media, Springer INdAM Series 55 (2023)

Cardoso, R., Vieira, J., Borges, I.: Water retention curve of biocemented sands using mip results. Appl. Sci. **12**, 10447 (2022). https://doi.org/10.3390/app122010447

Chen, Z., Huan, G., Ma, Y.: Computational methods for multiphase flows, porous media. Society for Industrial and Applied Mathematics (2006). https://doi.org/10.1137/1.9780898718942

Clarelli, F., Natalini, R., Nitsch, C., Santarelli, M. L.: A mathematical model for consolidation of building stones. Applied and Industrial Mathematics in Italy III: Selected Contributions from the 9th SIMAI Conference, Rome, Italy, 15-19 September, 2008, Vol. 82, World Scientific, (2009), p. 232

Backeberg, N.R., Iacoviello, F., Rittner, M., Mitchell, T.M., Jones, A.P., Day, R., Wheeler, J., Shearing, P.R., Vermeesch, P., Striolo, A.: Quantifying the anisotropy and tortuosity of permeable pathways in clay-rich mudstones using models based on X-ray tomography. Scientific Reports volume 7, Article number: 14838, (2017)

Battiato, G.: Le malte del centro storico di Catania, Mater. e Tec. Costr. Della Tradiz. Sicil. Doc. 16 Dell'Istituto Dipartimentale Di Archit, e Urban., Universitá di Catania, (1988), pp. 85–107

Bear, J.: Dynamics of flow in porous media. Dover, NY (1972)

Belfiore, C.M., Russa, M.F., Mazzoleni, P., Pezzino, A., Viccaro, M.: Technological study of "ghiara" mortars from the historical city centre of catania (eastern sicily, italy) and petro-chemical characterisation of raw materials, environ. Earth Sci. **61**, 995–1003 (2010)

Belfiore, C.M., Visalli, R., Ortolano, G., Barone, G., Mazzoleni, P.: A gis-based image processing approach to investigate the hydraulic behavior of mortars induced by volcanic aggregates. Construct. Build. Mater. **342**, 128063 (2022). https://doi.org/10.1016/J.CONBUILDMAT.2022.128063

Brooks, R. H., Corey, A.T.: Hydraulic properties of porous media, Hydrol. Pap. 3, 27 pp., Colo. State Univ., Fort Collins, (1964)

Charola, A.E., Wendler, E.: An overview of the water-porous building materials interactions. Restoration of Buildings and Monuments **21**(2–3), 55–65 (2015). https://doi.org/10.1515/rbm-2015-0006

de Boever, W., Bultreys, T., Derluyn, H., Van Hoorebeke, L., Cnudde, V.: Comparison between traditional laboratory tests, permeability measurements and ct-based fluid flow modelling for cultural heritage applications. Sci. Total Environ. **554–555**, 102–112 (2016)

Della Vecchia, G., Dieudonné, A.C., Jommi, C., Charlier, R.: Accounting for evolving pore size distribution in water retention models for compacted clays Int. J. Numer. Anal. Meth, Geomech (2014)

Aregba-Driollet, D., Diele, F., Natalini, R.: A mathematical model for the sulphur dioxide aggression to calcium carbonate stones: numerical approxima- tion and asymptotic analysis. SIAM J. Appl. Math. **64**(5), 1636–1667 (2004). https://doi.org/10.1137/S003613990342829X

Gleeson, T., Smith, L., Moosdorf, N., Hartmann, J., Durr, H.H., Manning, A.H., van Beek, L.P. H., Jellinek, A.M.: Mapping permeability over the surface of the Earth, Geophysical Research Letters, Vol. 38 (2), (2011)

Rumble, J.R.: CRC Handbook of Chemistry and Physics (99th ed.). Boca Raton, ed. (2018), FL: CRC Press. ISBN 978-1-138-56163-2

HyperPhysics website, http://hyperphysics.phy-astr.gsu.edu/hbase/hframe.html, Georgia State University

van Genuchten, M.T.: A closed-form equation for predicting the hydraulic conductivity of unsaturated soils. Soil Sci. Soc. Am. J. **44**, 892–898 (1980)

Zahasky, C., Benson, S.M.: Spatial and temporal quantification of spontaneous imbibition. Geophysical Research Letters, 46, (2019) https://doi.org/10.1029/2019GL084532

Zimmerman, R.W., Bodvarsson, G.S.: An approximate solution for one-dimensional absorption in unsaturated porous media. Water Resour. Res. **25**, 1422–1428 (1989)